

# Path Planning With Naive-Valley-Path Obstacle Avoidance and Global Map-Free\*

Miguel Ángel Muñoz-Bañón, Edison Velasco-Sánchez, Francisco A. Candelas and Fernando Torres, *Senior member, IEEE*

**Abstract**— In this paper, we present a complete Path Planning approach divided into two main categories: Global Path Planning (GPP) and Local Path Planning (LPP). Unlike most other works, the GPP layer, instead of complex and heavy maps, uses road and intersections graphs obtained directly from internet applications like OpenStreetMaps (OSM). This map-free GPP frees us from the common area-size restrictions. In the LPP layer, we use a novel Naive-Valley-Path method (NVP) to generate a local path avoiding obstacles in the road in an extremely-low execution time period. This approach exploits the concept of “valley” areas around local minima, i.e., the ones always away from obstacles. We demonstrate the robustness of the system in our research platform BLUE, driving autonomously across the University of Alicante Scientific Park for more than 20 km in a 12.33 ha area. Our vehicle avoids different static persistent and non-persistent obstacles in the road and even dynamic ones, such as vehicles and pedestrians. Code is available at [https://github.com/AUROVA-LAB/lib\\_planning](https://github.com/AUROVA-LAB/lib_planning).

## I. INTRODUCTION

One of the most important autonomous navigation tasks is to reach a certain target given the vehicle’s current pose. During this process, the vehicle is subject to constraints such as not colliding with any obstacle. This is a non-trivial task because the environment in which the vehicle navigates is usually complex, with many obstacles, and it requires the estimation of sequential intermediate goals. These goals are usually known as path. The process is widely named in the literature as Path Planning, and it is a multi-layer task that requires: knowledge of the environment to plan the best possible path [1], scene understanding to avoid obstacles during navigation [2], and generation of the control actions to fit the vehicle trajectory to the desired path [3]. Path Planning can be divided into two different categories [4], [5]: Global Path Planning (GPP) and Local Path Planning (LPP).

Global Path Planning (GPP) uses the global environmental representation to check possible paths to obtain the best one in terms of a cost function. In this case, the environment representation usually contains persistent static elements. For this reason, the calculated path will not be strictly the one the robot will follow because the non-persistent static obstacles and dynamic obstacles will force route to be re-planned. GPP techniques can be classified into the Graph Search

\*This work has been supported by the Spanish Goverment through the FPI grant PRE2019-088069 and the research project RTI2018-094279-B-100, as well as by the regional Valencian Community Goverment and the European Regional Development Fund (ERDF) through the grant ACIF/2019/088.

The authors are with the Group of Automation, Robotics and Computer Vision (AUROVA), University of Alicante, San Vicente del Raspeig S/N, Alicante, Spain. [miguelangel.munoz@ua.es](mailto:miguelangel.munoz@ua.es)

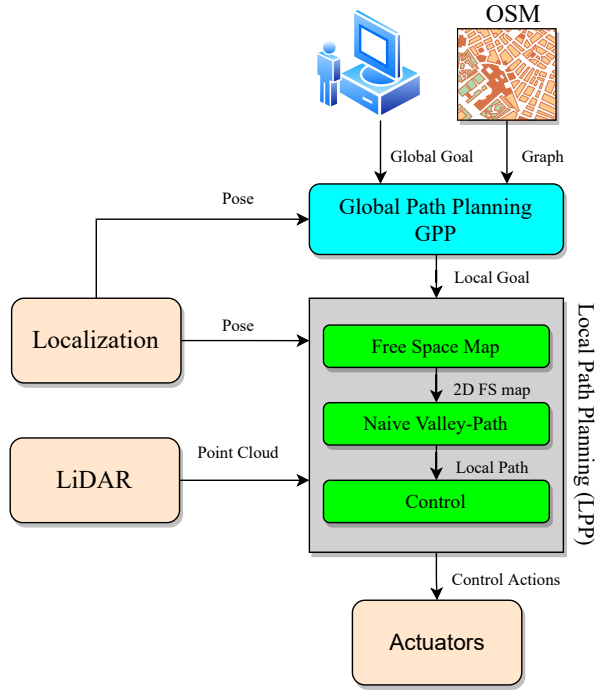


Fig. 1. The complete proposed Path Planning approach is organized hierarchically. First, the GPP gets information about global localization from the robot and global information about the environment from OSM to plan a global path. Then, the LPP module, using the presented Naive Valley-Path method, recalculates the local path to obtain the optimal way to follow.

Algorithm [6], [7], the Random Sampling Algorithm [8], [9], and the Intelligent Bionic Algorithm [10]. There are different classical graph search approaches in the literature, such as the Dijkstra algorithm [11], A\* algorithm [12], DFS algorithm [13], and BFS algorithm [14]. In [15], [16], [17], the authors improve the efficiency of the classical Graph Search Algorithm through a heuristic estimation, which reduces the number of searching grids and improves the searching efficiency. In most works, such as [18], [19], [20], the authors use grid maps as global environment representation. This entails an area-size limitation due to the memory limits and the weak global consistency of grid maps. Other works use available environment representation from the internet, such as top-view images [21] or OpenStreetMaps (OSM) information [22], [23].

Local Path Planning (LPP) uses the vehicle sensors, such as LiDAR or cameras, to understand the local environment. In this way, LPP can re-plan the path in function on the

obstacles closer to the vehicle. The LPP can be divided into static LPP [24], [25], which can detect only static objects (but not necessarily persistent), and dynamic LPP [26], [27], which tracks dynamic objects and consider his trajectories to replan the path. In the literature, there are many works based on classical algorithms for obtaining local paths, such as the Artificial Potential Field method [28], Fuzzy Logic Algorithm [29], Simulated Annealing Algorithm [30], a hybrid method combined with a genetic algorithm [31], and the particle algorithm [32], where the authors avoid the disadvantage that the solution is locally optimal. In the last years, there are many works focused on learning-based path planning methods [33]. The end-to-end self-driving methods compress the whole process of planning-control in one step based on a Convolutional Neural Network (CNN) [34], [35], [36], where the sensor data is the input of the network and where the control actions are the output. Another learning-based approach is the Reinforcement Learning (RL) [37], [38], [39], where the learning process occurs during vehicle navigation.

In this paper, we present a complete Path Planning approach divided into GPP and LPP. For the GPP layer, instead of maps, we use road information obtained from internet applications like OpenStreetMaps (OSM). This map-free GPP frees us from the area-size restrictions. In the LPP layer, we use a novel Naive-Valley-Path method (NVP) to generate a local path avoiding obstacles in the road. This approach exploits the concept of "valley" areas around local minima, i.e., the ones always away from obstacles. Due to the extremely-low execution time of our NVP algorithm, we can avoid dynamic obstacles such as vehicles and pedestrians, as we demonstrate experimentally. In this case, we cannot consider this method as completely dynamic because we do not use tracking to predict obstacles trajectories. But we can consider our approach as "semi-dynamic".

The rest of the paper is organized as follows: In Section II, we present an overview of the complete Path Planning method proposed. Then, local Path Planning and Global Path Planning modules are described in Sections III y IV, respectively. Next, in Sección V, we show the experimental results obtained using our own real robot BLUE. Finally, in Section VI, we present the main conclusions obtained from this work and possible future works.

## II. PROPOSED APPROACH ARCHITECTURE

In Fig. 1, we show the proposed approach, which is divided into different modules. The path planning is organized hierarchically. At the top-level, we compute the GPP that receives a graph obtained from the online application OSM, the final global goal provided by the user, and the pose obtained from the localization module. In this work, we assume that we have a georeferenced global localization. This is required to use the environment representation directly from OSM, which provides geolocalized information about roads and intersections. The GPP infers the best path through the graph using the A\* algorithm, and it gives as output a local goal, which is the nearest node of the calculated path.

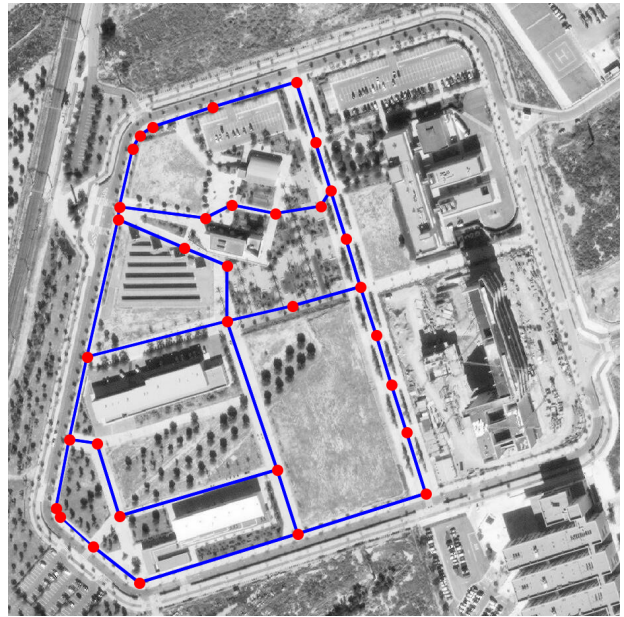


Fig. 2. Example of Graph used in the GPP module, in this case, extracted from the Scientific Park area in the University of Alicante. The red points describe the georeferenced position of nodes, while the blue lines represent the links that indicate a trafficable connection between nodes. We can extract the graph directly from current OSM data or create it manually in the same application.

This goal is an input for the LPP module. Moreover, the LPP receives as inputs the vehicle's localization and 3D LiDAR scans from the sensor. We divided the LPP hierarchically into three layers. In the "Free-space" calculation layer, we remove ground points and the points above the upper part of the vehicle. Then, we consider the rest of the points as obstacles that we use as borders of a free-space representation 2D map. In the Naive-Valley-Path NVP layer, we use the classical Potential Fields representation in the free-space map to infer a naive version of the best Valley-Path. Finally, we evaluate the possible actions, among ones without collision risk, that minimize the error between the vehicle pose and the local path.

In Section III and Section IV, we explain in more detail each module of the proposed approach.

## III. GLOBAL PATH PLANNING

At the Global Path Planning level, we need a representation of the environment. This representation can contain trees, buildings, traffic signals, roads, intersections, etc. If and only if we think at the GPP level, we can consider this representation of the environment as persistent static. Under this assumption, we decided to use the environment information from online applications such as OpenStreetMaps (OSM), which contains georeferenced persistent static elements. With this representation, we avoid the use of complex maps that usually give some problems, such as memory limitation, hard inference, and global inconsistencies produced by accumulated drifts.

We represent the environment as a graph, in which each node is a georeferenced point in a trafficable area, and

each link indicates that two points are connected through a passable road. In Fig. 2, we show an example of the graph plotted over the OSM map. We can obtain the graph representation directly by OSM downsampling the paths to lighten the process. Also, we can add nodes manually to areas that we know trafficable. Given graph  $\mathcal{G}$ , we find the best path between the nearest node to the vehicle's pose and the node nearest to the global goal provided by the user. For this search, we use the A\* algorithm. Once the path has been obtained, we store the pose of the nodes in a buffer. Finally, we send each node sequentially as a local goal to the LPP module as they are being reached. We consider a local goal reached when the Mahalanobis Distance (MD) [40] is less than a certain configurable threshold. Using this probabilistic distance, we can evaluate if a goal is reached depending on the covariance in the localization system. In this way, we can prevent severe deviation from reaching goals in case of considerable noisy localization.

#### IV. LOCAL PATH PLANNING

In this section, we describe the Local Path Planning module, which is divided hierarchically into three levels. This module aims to infer the final control actions to send to the vehicle's actuators. Also, in this process, we use the LiDAR sensor to avoid possible obstacles in the local goal-reaching.

##### A. Obstacles and Free-space Calculation

We consider as obstacles the points in a LiDAR point cloud that are not part of the surface on which the vehicle circulates, i.e., the ones that are representing objects above the ground, or even points under the ground, such as descending steps. Besides, we consider obstacles only the points that are under the upper part of the vehicle, which is the collision risk fringe.

Given this definition, we need to detect the ground points to consider obstacles to the rest. In large part of the scenarios, we observed the ground surface is usually flat. Hence, we make a plane assumption using the LiDAR point cloud  $\mathcal{P}$  for a nonlinear Least-Squares optimization (based on [41]) to find the optimal ground plane parameters (1) that minimize the accumulated point-to-plane error for all points  $\mathbf{p} \in \mathcal{P}$ :

$$\mathbf{p}^* = \arg \min_{\mathbf{p}^*} \sum_{\mathbf{p} \in \mathcal{P}} \rho (||\mathbf{e}(\mathbf{p}^*, \mathbf{p})||^2) \quad (1)$$

Where  $\mathbf{e}(\mathbf{p}^*, \mathbf{p})$  denotes the distance vector between  $\mathbf{p}$  and its plane projection point. The loss function  $\rho$  is chosen to be the Cauchy loss with a small scale to robustly against outliers. We then remove all points from the point set with a distance below a threshold to the  $\mathbf{p}^*$  plane. To consider possible slope changes in the terrain, we apply this threshold proportionally to the distance to the sensor center. Finally, we displace the plane in the  $z$  axis to the upper part of the vehicle, and we then remove the points over this second plane. The points that remain in  $\mathcal{P}$  after this process are what we consider obstacles in a new point cloud  $\mathcal{P}^o$ . In Fig. 3 a), we show an example of  $\mathcal{P}^o$  projected in a 2D plane.

Starting from  $\mathcal{P}^o$ , we build a 2D representation of the free space. We define free space as the area inside a polygon where the contours are obstacle points. To build the polygon, first, we represent  $\mathcal{P}^o$  as a grid using a spherical representation. The rows and columns in this grid represent the elevation and azimuth angles, respectively, and the value in each cell is the range value. The cells with no point information have an empty value. Then, we sweep the columns of the grid. If the column contains points, we choose the one with the lowest range value, and we project it in a 2D cartesian representation ( $xy$ ). The points selected are the ones that form the free-space polygon. In Fig. 3 b), we show an example of free-space map.

##### B. Valley-Path Calculation

Once we know the free space around the vehicle, we need to determine a path in that space to reach the local goal. For this, we use a representation of free space based on the classical Artificial Potential Fields (APF). We consider the local goal as an attractor  $p_a$  and the nearest obstacle point as a repulsor  $p_r$ . Then, for each discrete point  $p_{ij}$  in the free space, we obtain the potential as follows:

$$f_{ij} = \frac{w_r}{(p_{ij} - p_r)^{\gamma_r}} - \frac{w_a}{(p_{ij} - p_a)^{\gamma_a}} \quad (2)$$

Where  $w_a$  and  $w_r$  are the weight of the attractive potential and the repulsive potential, respectively. And where  $\gamma_a$  and  $\gamma_r$  are the parameters to control the decay of potential respect the distance. In Fig. 3 c), we show an example of our APF-based representation for one LiDAR scan. The direction of the gradient of the representation shown in Fig. 3 c) is used in classical APF to infer the control actions of the robot. Nonetheless, this algorithm has the flaw of suffering the effect of local minima. In our approach, we use this representation to infer a path that passes through local minima areas until it reaches the global minima. By definition, these areas of local minima are always away from obstacles. We name these areas as "valleys" from now on. To segment the valleys in the map, we assume that the values of the magnitude of the gradient at point  $f_{ij}$  close to zero can be considered a point in a valley. Then, each point that satisfies (3) is labeled as a valley.

$$|\nabla f_{ij}| < \xi \quad (3)$$

Where  $\xi$  is a configurable threshold. Fig. 3 d) shows an example of a segmented valley. In the example, the darkest points mark the lowest magnitude of gradient points. We can see that this representation define clearly possible Valley-Paths.

In order to infer a Valley-Path between the sensor pose and the global minimum in the map, we could use some methods inside valleys such as geodesic distance [42]. However, this approach has the flaw of being excessively time-consuming in computational terms. For this reason, we develop a "naive" versión of this Valley-Path calculation that we explain in Section IV-C.

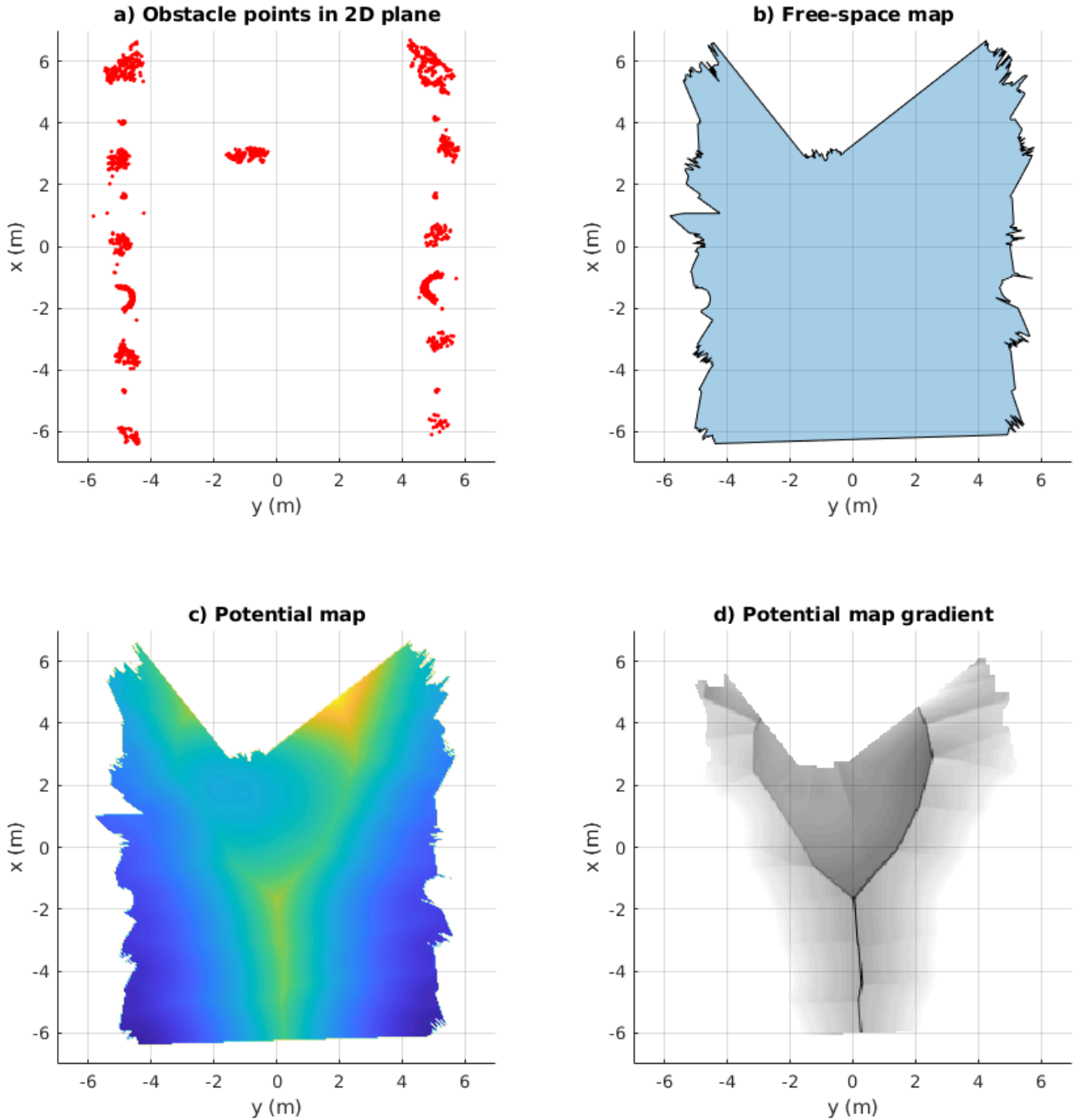


Fig. 3. Different 2D representation of LiDAR information for Valley-Path calculation: a) Projection in a 2D plane of obstacles point cloud  $\mathcal{P}^o$ . b) Free-space map, where the blue area represents the space free of obstacles. c) Potential representation defined in (2). d) Inverted representation of the gradient magnitude of c), which shows clear possible paths in the valley areas.

### C. Naive Version of the Valley-Path Calculation

Given a circle around the sensor pose, for each polar coordinate  $(r, \varphi_i)$  we can apply the expression (4), which is the 1D version of (2).

$$f_i = \frac{w_r}{(p_i - p_r)^{\gamma_r}} - \frac{w_a}{(p_i - p_a)^{\gamma_a}} \quad (4)$$

If we represent this 1-dimensional signal as a magnitude of the gradient, we can label as valley points the ones that

satisfy (3). We can do the same process in inner concentric circles. In this way, we can make the following **naive assumption**: given a valley point  $p_i^{c_1}$  in a circle  $c_1$ , and given the nearest valley point  $p_n^{c_2}$  in an inner circle  $c_2$ , the line that connects  $p_i^{c_1}$  with  $p_n^{c_2}$  is considered part of a path in the same valley. The subscript  $n$  means the index of the nearest valley point.

Under this assumption, given a set of  $N$  circles  $(c_0, c_1, \dots, c_N)$ , we can define the Naive-Valley-Path (NVP)

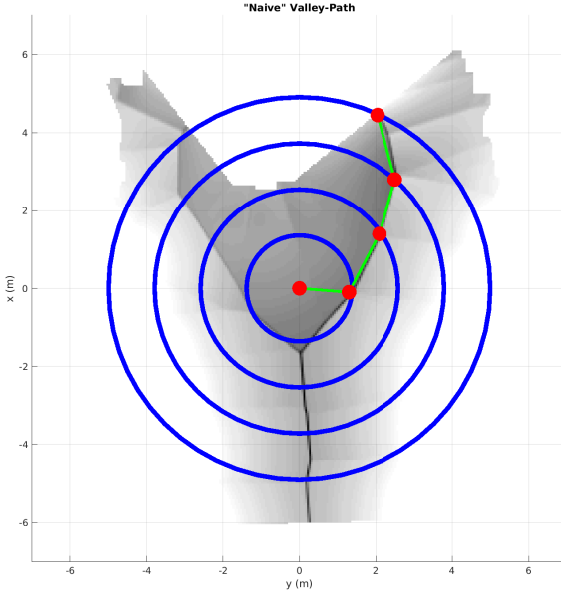


Fig. 4. The Naive-Valley-Path (NVP) Calculation. The red points are the ones that form the local path. The green connections describe the **naive assumption** and define the angle of the points. For the sake of clarity, this representation shows the NVP superpose with non-naive representation.

as a set of join points  $(p_n^{c_0}, p_n^{c_1}, \dots, p_n^{c_N})$  in which each element is connected with the nearest previous one. The first point  $p_n^{c_0}$  is the valley point in the external circle nearest to the local goal  $p_a$ . As  $N$  increases, the result can converge to the non-naive version of the Valley-Path calculation. The process described in this section is executed each time a LiDAR scan is received, i.e., the local path is recalculated in each iteration. In Fig. 4 we show an example of NVP and the circles used for the inference. To more clearly show how NVP follows the valley areas, in Fig. 4 we superpose it to the original non-naive representation.

#### D. Control Actions Calculation

Finally, in the lower-level layer, given a local path, we obtain the control actions  $u = (v, \alpha)$  that are the output of the LPP module.  $v$  is the linear absolute velocity of the vehicle, and  $\alpha$  is the steering position. For this, we compute a prediction of trajectories for any possible  $\alpha$  at the front and rear directions (Fig. 5). Given a sampled  $i$ -th trajectories and the size of the vehicle, we evaluate the collision risk for each one. If some part of the vehicle (with an added security margin) is out from the free-space map at any point of a  $i$ -th trajectory, the whole trajectory is considered to be at risk of collision, and it associated  $\alpha_i$  is discarded as possible variable for the control action. Fig. 5 shows an example of estimated trajectories where the red ones are labeled as collision-risk.

Once we have the collision-free trajectories (green ones in Fig. 5), we evaluate the error between each  $j$ -th pose in a  $i$ -th trajectory  $x_{ij}$  and each  $k$ -th pose  $p_k$  in the complete

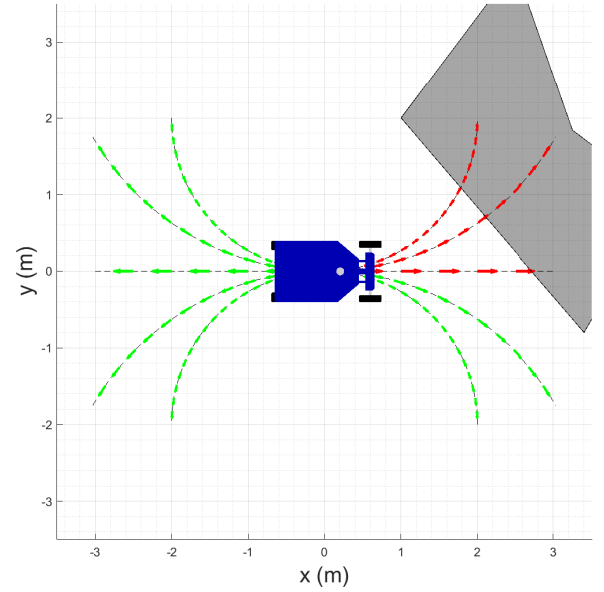


Fig. 5. The arcs represent the possible trajectories of control actions  $u_i$ . The red ones are the collision-risk trajectories, and their corresponding control actions are discarded. In contrast, the green ones are collision-free.

local path. We compute error as follows:

$$e_{ijk} = c_p (|x_{ij}^p - p_k^p|) + c_o (x_{ij}^o - p_k^o), \forall i, \forall j, \forall k \quad (5)$$

$$i^* = \min(e_{ijk}), \forall i, \forall j, \forall k \quad (6)$$

Where superscript and subscript  $p$  and  $o$  mean position and orientation, respectively, and where  $c_p$  and  $c_o$  are configurable constants to relate the different magnitudes. The result  $i^*$  is the index for the control action variable  $\alpha_i$ . The variable  $v$  of the control action is computed as follows:

$$v = v_{max} - |\alpha_i| \frac{v_{max} - v_{min}}{\alpha_{max}} \quad (7)$$

Where  $v_{max}$ ,  $v_{min}$ , and  $\alpha_{max}$ , are configurable parameters that depends on the vehicle's characteristics. In case of no collision-free trajectories, control action variables are  $\alpha = 0$  and  $v = 0$ .

## V. EXPERIMENTS

We evaluated the Path Planning method presented in this paper in our research platform *BLUE: roBot for Localization in Unstructured Environments* [43]. This robot includes actuators for speed and steering, traction and steering encoders, IMU, GPS, and LiDAR 3D Velodyne VLP16. All them integrated into *Robot Operating System* (ROS). The developed software is included in the framework for fast experimental testing presented in [44]. We use a fusion of encoders, IMU, and GPS as a localization system that provides localization in global coordinates. The error of this system is subject to the error in GPS, which in our experimental sessions

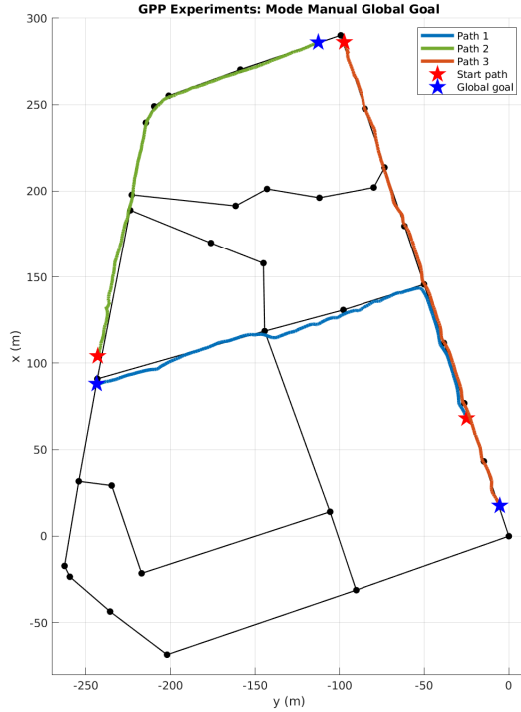


Fig. 6. Three examples of global goal-reaching. The red marks indicate the vehicle location when a goal was sent, and the blue marks indicate the sent goal locations.

reaches peaks until 15 meters of variance in the  $xy$  plane. Our Path Planning method demonstrated robustness against these localization measurement errors.

We carried out the experiments in the Scientific Park at the University of Alicante. This area contains parking lots and pedestrian walkable areas with trees, benches, and curbs. We show this area in Fig. 2. We drove our vehicle autonomously across this 12.33 ha area during the experimental sessions of more than 20 km with static obstacles in the road and dynamic ones, such as cars and pedestrians.

#### A. Experimental Results: Global goal-reaching

Given the graph shown in Fig. 2, built using the OSM application, we tested the global goal-reaching by sending different goals repetitively. In Fig. 6, we show three autonomous driving path examples obtained after sending global goals. The red marks indicate the vehicle location when a goal was sent, and the blue marks indicate the sent goal location. We can see that the vehicle always reaches the target by traveling the shortest way.

#### B. Experimental Results: Closed-loop paths

To test the repetitiveness of the paths, we set up an experimental session by defining different paths as a closed-loop. The paths are composed of arrays of local goals (nodes in the graph in Fig. 2) reached sequentially. When the last

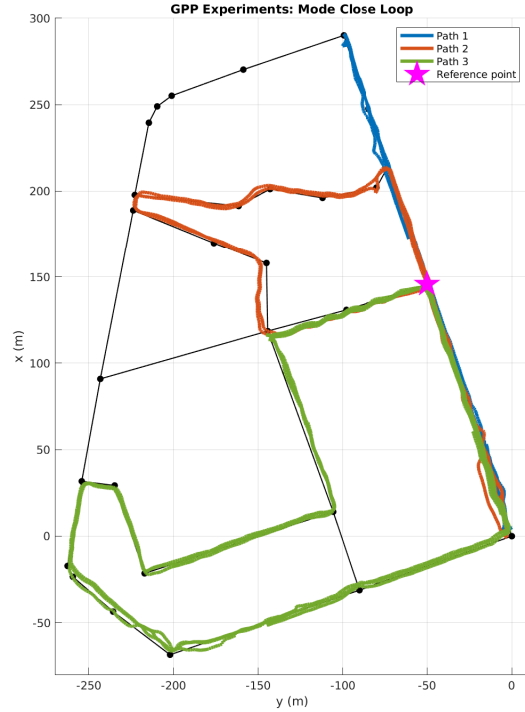


Fig. 7. Three examples of paths in autonomous navigation in closed-loop function mode. The star marks the reference point to measure the results shown in Table I.

local goal is reached, the process continues from the first local goal in the array.

Fig. 7 shows three examples of closed-loop paths, where we drove the vehicle three laps for each path autonomously. Path 1 is a straight-way loop, and this entails that the vehicle realizes two U-turns maneuvers in each lap. Path 2 also contains one U-turn maneuver in each lap (node in the point  $x = 0$  and  $y = 0$ ). Path 3 is "circular" type and doesn't require U-turns maneuvers. As we can see in Fig. 7, the path is not completely repeated, e. g., path 1 in  $x = [200, 250]$ , or path 2 around  $x = 0$  and  $y = 0$ . The GPS variable errors produce these cases. However, in all the high-error cases, the vehicle always circulates in a trafficable road, reaching the local goals successfully.

In Table I, we show quantitative results in the test of repeatability. This table shows the error obtained when a specific local goal (marked in Fig. 7) is considered reached. We also specify the variance given by the localization system. We can see that the error in reaching the point is correlated with the error in the localization system. Finally, we show the mean execution time ( $\mu_{\text{time}}$ ) of the whole process for each iteration of the proposed Path Planning strategy. We can see that we could use sensors even of 40/50 Hz. This specification makes our method able to use in reasonable fast applications.

TABLE I

QUANTITATIVE RESULTS IN THE TEST OF REPEATABILITY FOR THE PP METHOD.

Path	Loop	Error (m)	$\sigma^2$ (m)	$\mu_{time}$ (ms)
1	1	1.99	15.61	19.5
	2	0.28	3.32	20.5
	3	1.11	3.29	19.8
2	1	0.15	6.32	20.0
	2	1.69	6.61	21.3
	3	1.34	7.19	19.5
3	1	1.21	4.28	19.6
	2	1.47	3.77	18.6
	3	0.77	0.85	18.2

### C. Experimental Results: Obstacle avoidance

During the autonomous navigation done during the experiments shown before, we also tested obstacle avoidance. Fig. 8 shows an image sequence of repeated pedestrian avoidance, where the time evolution is from left to right. We enumerate these images from 1 to 5. In image 1, we can see a pedestrian running to cross the vehicle's trajectory. The vehicle rectifies his local path, but the pedestrian stops just in the front of the vehicle (image 2). In image 3, the vehicle maneuvers to avoid the pedestrian, but then the pedestrian stops in front of the vehicle again (image 4). Finally, in image 5, the vehicle avoids the pedestrian and continues the travel to reach the goal.

In Fig. 9, we show another example of obstacle avoidance: a car in the parking. In this case, the vehicle follows a straight trajectory, but a car drive to cross this trajectory. However, due to the NVP Local Path Planning module, the vehicle recalculates the path to avoid this dynamic obstacle, as shown in the sequence of Fig. 9.

## VI. CONCLUSIONS AND FUTURE WORKS

In this paper, we have presented a complete Path Planning method divided hierarchically into two modules: Global Path Planning and Local Path Planning. The first module allows to plan paths at a high level without an exhaustive representation of the environment, leaving the application free of area size constraints. The LPP module allows, in a fast way, the avoidance of obstacles in the path using the concept of Valley-Paths, which are the local paths that follow the local minima areas. We demonstrate the potential of the method experimentally to reach global goals and its robustness against localization errors. Also, we demonstrate how our NVP based LPP achieves fast and robust obstacle avoidance even in dynamic cases, such as cars and pedestrians.

As future works, we plan to use an online interface with OSM to make a dynamic graph for the GPP. In this way, we could navigate in an exploration mode into completely unknown areas. Also, we plan to use more sophisticated perception techniques, such a Convolutional Neural Networks (CNN), to classify obstacles in the environment.

## REFERENCES

- [1] B. Ichter, J. Harrison, and M. Pavone, "Learning sampling distributions for robot motion planning," in *2018 IEEE International Conference on Robotics and Automation (ICRA)*. IEEE, 2018, pp. 7087–7094.
- [2] J.-R. Xue, J.-W. Fang, and P. Zhang, "A survey of scene understanding by event reasoning in autonomous driving," *International Journal of Automation and Computing*, vol. 15, no. 3, pp. 249–266, 2018.
- [3] S. G. Tzafestas, "Mobile robot control and navigation: A global overview," *Journal of Intelligent & Robotic Systems*, vol. 91, no. 1, pp. 35–58, 2018.
- [4] K. Cai, C. Wang, J. Cheng, C. W. De Silva, and M. Q.-H. Meng, "Mobile robot path planning in dynamic environments: A survey," *arXiv preprint arXiv:2006.14195*, 2020.
- [5] J. Guzzi, R. O. Chavez-Garcia, M. Nava, L. M. Gambardella, and A. Giusti, "Path planning with local motion estimations," *IEEE Robotics and Automation Letters*, vol. 5, no. 2, pp. 2586–2593, 2020.
- [6] D. Kularatne, S. Bhattacharya, and M. A. Hsieh, "Optimal path planning in time-varying flows using adaptive discretization," *IEEE Robotics and Automation Letters*, vol. 3, no. 1, pp. 458–465, 2017.
- [7] P. C. Chen and Y. K. Hwang, "Sandros: a dynamic graph search algorithm for motion planning," *IEEE Transactions on Robotics and Automation*, vol. 14, no. 3, pp. 390–403, 1998.
- [8] L. Schmid, M. Pantic, R. Khanna, L. Ott, R. Siegwart, and J. Nieto, "An efficient sampling-based method for online informative path planning in unknown environments," *IEEE Robotics and Automation Letters*, vol. 5, no. 2, pp. 1500–1507, 2020.
- [9] S. Karaman and E. Frazzoli, "Sampling-based algorithms for optimal motion planning," *The international journal of robotics research*, vol. 30, no. 7, pp. 846–894, 2011.
- [10] T. Chen, "A simulative bionic intelligent optimization algorithm: artificial searching swarm algorithm and its performance analysis," in *2009 International Joint Conference on Computational Sciences and Optimization*, vol. 2. IEEE, 2009, pp. 864–866.
- [11] S. Broumi, A. Bakal, M. Talea, F. Smarandache, and L. Vladareanu, "Applying dijkstra algorithm for solving neutrosophic shortest path problem," in *2016 International conference on advanced mechatronic systems (ICAMEchS)*. IEEE, 2016, pp. 412–416.
- [12] F. Duchoň, A. Babinec, M. Kajan, P. Beňo, M. Florek, T. Fico, and L. Jurišica, "Path planning with modified a star algorithm for a mobile robot," *Procedia Engineering*, vol. 96, pp. 59–69, 2014.
- [13] M. Guo, K. H. Johansson, and D. V. Dimarogonas, "Revising motion planning under linear temporal logic specifications in partially known workspaces," in *2013 IEEE International Conference on Robotics and Automation*. IEEE, 2013, pp. 5025–5032.
- [14] J. Yu and S. M. LaValle, "Planning optimal paths for multiple robots on graphs," in *2013 IEEE International Conference on Robotics and Automation*. IEEE, 2013, pp. 3612–3617.
- [15] X. Dai, S. Long, Z. Zhang, and D. Gong, "Mobile robot path planning based on ant colony algorithm with a\* heuristic method," *Frontiers in neurorobotics*, vol. 13, p. 15, 2019.
- [16] S. Li, W. Su, R. Huang, and S. Zhang, "Mobile robot navigation algorithm based on ant colony algorithm with a\* heuristic method," in *2020 4th International Conference on Robotics and Automation Sciences (ICRAS)*. IEEE, 2020, pp. 28–33.
- [17] Y. Li, D. Dong, and X. Guo, "Mobile robot path planning based on improved genetic algorithm with a-star heuristic method," in *2020 IEEE 9th Joint International Information Technology and Artificial Intelligence Conference (ITAIC)*, vol. 9. IEEE, 2020, pp. 1306–1311.
- [18] E. Tsardoulias, A. Iliakopoulou, A. Kargakos, and L. Petrou, "A review of global path planning methods for occupancy grid maps regardless of obstacle density," *Journal of Intelligent & Robotic Systems*, vol. 84, no. 1, pp. 829–858, 2016.
- [19] Y. Chen, G. Bai, Y. Zhan, X. Hu, and J. Liu, "Path planning and obstacle avoiding of the usv based on improved aco-afp hybrid algorithm with adaptive early-warning," *IEEE Access*, 2021.
- [20] J. Laconte, A. Kasmi, F. Pomerleau, R. Chapuis, L. Malaterre, C. Debaïn, and R. Aufrère, "Lambda-field: A continuous counterpart of the bayesian occupancy grid for risk assessment and safe navigation," *arXiv preprint arXiv:2011.08045*, 2020.
- [21] V.-D. Hoang, D. C. Hernández, J. Hariyono, and K.-H. Jo, "Global path planning for unmanned ground vehicle based on road map images," in *2014 7th International Conference on Human System Interactions (HSI)*. IEEE, 2014, pp. 82–87.



Fig. 8. **Obstacle avoidance experiments:** Example of pedestrian avoidance in an image sequence. A pedestrian crosses the vehicle trajectory twice (images 2 and 4 from left to right). In both cases, the vehicle avoids this dynamic obstacle.



Fig. 9. **Obstacle avoidance experiments:** Example of car avoidance in an image sequence. The vehicle circulates in a straight-line way and modifies its trajectory when a car crosses its path.

- [22] A. Artuñedo, J. Godoy, and J. Villagra, “A decision-making architecture for automated driving without detailed prior maps,” in *2019 IEEE Intelligent Vehicles Symposium (IV)*. IEEE, 2019, pp. 1645–1652.
- [23] B. Suger and W. Burgard, “Global outer-urban navigation with openstreetmap,” in *2017 IEEE International Conference on Robotics and Automation (ICRA)*. IEEE, 2017, pp. 1417–1422.
- [24] Z. B. Garip, G. Atali, D. Karayel, and S. S. Ozkan, “Path planning for multiple mobile robots in static environment using hybrid algorithm,” in *2018 2nd International Symposium on Multidisciplinary Studies and Innovative Technologies (ISMSIT)*. IEEE, 2018, pp. 1–4.
- [25] T. XiangRong, Z. Yukun, and J. XinXin, “Improved a-star algorithm for robot path planning in static environment,” in *Journal of Physics: Conference Series*, vol. 1792, no. 1. IOP Publishing, 2021, p. 012067.
- [26] J. Ji, A. Khajepour, W. W. Melek, and Y. Huang, “Path planning and tracking for vehicle collision avoidance based on model predictive control with multiconstraints,” *IEEE Transactions on Vehicular Technology*, vol. 66, no. 2, pp. 952–964, 2016.
- [27] X. Hu, L. Chen, B. Tang, D. Cao, and H. He, “Dynamic path planning for autonomous driving on various roads with avoidance of static and moving obstacles,” *Mechanical Systems and Signal Processing*, vol. 100, pp. 482–500, 2018.
- [28] A. Le Gouguec, A. Kemeny, A. Berthoz, and F. Merienne, “Artificial potential field simulation framework for semi-autonomous car conception,” *Science Arts and Metiers*, 2017.
- [29] A. Bakdi, A. Hentout, H. Boutami, A. Maoudj, O. Hachour, and B. Bouzouia, “Optimal path planning and execution for mobile robots using genetic algorithm and adaptive fuzzy-logic control,” *Robotics and Autonomous Systems*, vol. 89, pp. 95–109, 2017.
- [30] T. Turker, O. K. Sahingoz, and G. Yilmaz, “2d path planning for uavs in radar threatening environment using simulated annealing algorithm,” in *2015 International Conference on Unmanned Aircraft Systems (ICUAS)*. IEEE, 2015, pp. 56–61.
- [31] P. Paulo, F. Branco, J. de Brito, and A. Silva, “Buildingslife—the use of genetic algorithms for maintenance plan optimization,” *Journal of cleaner production*, vol. 121, pp. 84–98, 2016.
- [32] M. Petrović, N. Vuković, M. Mitić, and Z. Miljković, “Integration of process planning and scheduling using chaotic particle swarm optimization algorithm,” *Expert systems with Applications*, vol. 64, pp. 569–588, 2016.
- [33] J. Cheng, H. Cheng, M. Q.-H. Meng, and H. Zhang, “Autonomous navigation by mobile robots in human environments: A survey,” in *2018 IEEE International Conference on Robotics and Biomimetics (ROBIO)*. IEEE, 2018, pp. 1981–1986.
- [34] M. Bojarski, D. Del Testa, D. Dworakowski, B. Firner, B. Flepp, P. Goyal, L. D. Jackel, M. Monfort, U. Muller, J. Zhang *et al.*, “End to end learning for self-driving cars,” *arXiv preprint arXiv:1604.07316*, 2016.
- [35] P. Cai, S. Wang, Y. Sun, and M. Liu, “Probabilistic end-to-end vehicle navigation in complex dynamic environments with multimodal sensor fusion,” *IEEE Robotics and Automation Letters*, vol. 5, no. 3, pp. 4218–4224, 2020.
- [36] B. Riviere, W. Höning, Y. Yue, and S.-J. Chung, “Glas: Global-to-local safe autonomy synthesis for multi-robot motion planning with end-to-end learning,” *IEEE Robotics and Automation Letters*, vol. 5, no. 3, pp. 4249–4256, 2020.
- [37] X. Pan, Y. You, Z. Wang, and C. Lu, “Virtual to real reinforcement learning for autonomous driving,” *arXiv preprint arXiv:1704.03952*, 2017.
- [38] B. Wang, Z. Liu, Q. Li, and A. Prorok, “Mobile robot path planning in dynamic environments through globally guided reinforcement learning,” *IEEE Robotics and Automation Letters*, vol. 5, no. 4, pp. 6932–6939, 2020.
- [39] A. Amini, I. Gilitschenski, J. Phillips, J. Moseyko, R. Banerjee, S. Karaman, and D. Rus, “Learning robust control policies for end-to-end autonomous driving from data-driven simulation,” *IEEE Robotics and Automation Letters*, vol. 5, no. 2, pp. 1143–1150, 2020.
- [40] R. De Maesschalck, D. Jouan-Rimbaud, and D. L. Massart, “The mahalanobis distance,” *Chemometrics and intelligent laboratory systems*, vol. 50, no. 1, pp. 1–18, 2000.
- [41] S. Wirges, C. Stiller, and F. Hartenbach, “Evidential occupancy grid map augmentation using deep learning,” in *2018 IEEE intelligent vehicles symposium (IV)*. IEEE, 2018, pp. 668–673.
- [42] F. Ortiz, S. Puente, and F. Torres, “Mathematical morphology and binary geodesy for robot navigation planning,” in *International Conference on Pattern Recognition and Image Analysis*. Springer, 2005, pp. 118–126.
- [43] I. del Pino, M. A. Munoz-Banon, S. Cova-Rocamora, M. A. Contreras, F. A. Candelas, and F. Torres, “Deeper in blue,” *Journal of Intelligent & Robotic Systems*, vol. 98, no. 1, pp. 207–225, 2020.
- [44] M. Á. Muñoz-Bañón, I. del Pino, F. A. Candelas, and F. Torres, “Framework for fast experimental testing of autonomous navigation algorithms,” *Applied Sciences*, vol. 9, no. 10, p. 1997, 2019.